EUROPEAN ORGANIZATION FOR NUCLEAR RESEARCH

CERN–PH-EP-2006-016

16 May 2006

Masses, Lifetimes and Production Rates of Ξ^- and $\overline{\Xi}^+$ at LEP 1

DELPHI Collaboration

Abstract

Measurements of the Ξ^- and $\overline{\Xi}^+$ masses, mass differences, lifetimes and lifetime differences are presented. The $\overline{\Xi}^+$ sample used is much larger than those used previously for such measurements. In addition, the Ξ production rates in $Z\to b\bar{b}$ and $Z\to q\bar{q}$ events are compared and the position ξ^* of the maximum of the ξ distribution in $Z\to q\bar{q}$ events is measured.

(Accepted by Physics Letters B)

J.Abdallah[25], P.Abreu[22], W.Adam[51], P.Adzic[11], T.Albrecht[17], T.Alderweireld[2], R.Alemany-Fernandez[8], T.Allmendinger[17], P.P.Allport[23], U.Amaldi[29], N.Amapane[45], S.Amato[48], E.Anashkin[36], A.Andreazza[28], S.Andringa[22], N.Anjos[22], P.Antilogus[25], W-D.Apel[17], Y.Arnoud[14], S.Ask[26], B.Asman[44], J.E.Augustin[25], A.Augustinus[8], P.Baillon[8], A.Ballestrero[46], P.Bambade[20], R.Barbier[27], D.Bardin[16], G.J.Barker[17], A.Baroncelli[39], M.Battaglia[8], M.Baubillier[25], K-H.Becks[53], M.Begalli[6], A.Behrmann[53], E.Ben-Haim[20], N.Benekos[32], A.Benvenuti[5], C.Berat[14], M.Berggren[25], L.Bernt zon[44], D.Bertrand[2], M.Besancon[40], N.Besson[40], D.Bloch[9], M.Blom[31], M.Bluj[52], M.Bonesini[29], M.Boonekamp[40], P.S.L.Booth†[23], G.Borisov[21], O.Botner[49], B.Bouquet[20], T.J.V.Bowcock[23], I.Boyko[16], M.Bracko[43], R.Brenner[49], E.Brodet[35], P.Bruckman[18], J.M.Brunet[7], B.Buschbeck[51], P.Buschmann[53], M.Calvi[29], T.Camporesi[8], V.Canale[38], F.Carena[8], N.Castro[22], F.Cavallo[5], M.Chapkin[42], Ph.Charpentier[8], P.Checchia[36], R.Chierici[8], P.Chliapnikov[42], J.Chudoba[8], S.U.Chung[8], K.Cieslik[18], P.Collins[8], R.Contri[13], G.Cosme[20], F.Cossutti[47], M.J.Costa[50], D.Crennell[37], J.Cuevas[34], J.D'Hondt[2], J.Dalmau[44], T.da Silva[48], W.Da Silva[25], G.Della Ricca[47], A.De Angelis[47], W.De Boer[17], C.De Clercq[2], B.De Lotto[47], N.De Maria[45], A.De Min[36], L.de Paula[48], L.Di Ciaccio[38], A.Di Simone[39], K.Doroba[52], J.Drees[53,8], G.Eigen[4], T.Ekelof[49], M.Ellert[49], M.Elsing[8], M.C.Espirito Santo[22], G.Fanourakis[11], D.Fassouliotis[11,3], M.Feindt[17], J.Fernandez[41], A.Ferrer[50], F.Ferro[13], U.Flagmeyer[53], H.Foeth[8], E.Fokitis[32], F.Fulda-Quenzer[20], J.Fuster[50], M.Gandelman[48], C.Garcia[50], Ph.Gavillet[8], E.Gazis[32], R.Gokieli[8,52], B.Golob[43], G.Gomez-Ceballos[41], P.Goncalves[22], E.Graziani[39], G.Grosdidier[20], K.Grzelak[52], J.Guy[37], C.Haag[17], A.Hallgren[49], K.Hamacher[53], K.Hamilton[35], S.Haug[33], F.Hauler[17], V.Hedberg[26], M.Hennecke[17], H.Herr†[8], J.Hoffman[52], S-O.Holmgren[44], P.J.Holt[8], M.A.Houlden[23], J.N.Jackson[23], G.Jarlskog[26], P.Jarry[40], D.Jeans[35], E.K.Johansson[44], P.D.Johansson[44], P.Jonsson[27], C.Joram[8], L.Jungermann[17], F.Kapusta[25], S.Katsanevas[27], E.Katsoufis[32], G.Kernel[43], B.P.Kersevan[8,43], U.Kerzel[17], B.T.King[23], N.J.Kjaer[8], P.Kluit[31], P.Kokkinias[11], C.Kourkoumelis[3], O.Kouznetsov[16], Z.Krumstein[16], M.Kucharczyk[18], J.Lamsa[1], G.Leder[51], F.Ledroit[14], L.Leinonen[44], R.Leitner[30], J.Lemonne[2], V.Lepeltier[20], T.Lesiak[18], W.Liebig[53], D.Liko[51], A.Lipniacka[44], J.H.Lopes[48], J.M.Lopez[34], D.Loukas[11], P.Lutz[40], L.Lyons[35], J.MacNaughton[51], A.Malek[53], S.Maltezos[32], F.Mandl[51], J.Marco[41], R.Marco[41], B.Marechal[48], M.Margoni[36], J-C.Marin[8], C.Mariotti[8], A.Markou[11], C.Martinez-Rivero[41], J.Masik[12], N.Mastroyiannopoulos[11], F.Matorras[41], C.Matteuzzi[29], F.Mazzucato[36], M.Mazzucato[36], R.Mc Nulty[23], C.Meroni[28], E.Migliore[45], W.Mitaroff[51], U.Mjoernmark[26], T.Moa[44], M.Moch[17], K.Moenig[8,10], R.Monge[13], J.Montenegro[31], D.Moraes[48], S.Moreno[22], P.Morettini[13], U.Mueller[53], K.Muenich[53], M.Mulders[31], L.Mundim[6], W.Murray[37], B.Muryn[19], G.Myatt[35], T.Myklebust[33], M.Nassiakou[11], F.Navarria[5], K.Nawrocki[52], R.Nicolaidou[40], M.Nikolenko[16,9], P.Niss[44], A.Oblakowska-Mucha[19], V.Obraztsov[42], A.Olshevski[16], A.Onofre[22], R.Orava[15], K.Osterberg[15], A.Ouraou[40], A.Oyanguren[50], M.Paganoni[29], S.Paiano[5], J.P.Palacios[23], H.Palka[18], Th.D.Papadopoulou[32], L.Pape[8], C.Parkes[24], F.Parodi[13], U.Parzefall[8], A.Passeri[39], O.Passon[53], L.Peralta[22], V.Perepelitsa[50], A.Perrotta[5], A.Petrolini[13], J.Piedra[41], L.Pieri[39], F.Pierre[40], M.Pimenta[22], E.Piotto[8], T.Podobnik[43], V.Poireau[8], M.E.Pol[6], G.Polok[18], V.Pozdniakov[16], N.Pukhaeva[2,16], A.Pullia[29], J.Rames[12], A.Read[33], P.Rebecchi[8], J.Rehn[17], D.Reid[31], R.Reinhardt[53], P.Renton[35], F.Richard[20], J.Ridky[12], M.Rivero[41], D.Rodriguez[41], A.Romero[45], P.Ronchese[36], P.Roudeau[20], T.Rovelli[5], V.Ruhlmann-Kleider[40], D.Ryabtchikov[42], A.Sadovsky[16], L.Salmi[15], J.Salt[50], C.Sander[17], A.Savoy-Navarro[25], U.Schwickerath[8], R.Sekulin[37], M.Siebel[53], A.Sisakian[16], G.Smadja[27], O.Smirnova[26], A.Sokolov[42], A.Sopczak[21], R.Sosnowski[52], T.Spassov[8], M.Stanitzki[17], A.Stocchi[20], J.Strauss[51], B.Stugu[4], M.Szczekowski[52], M.Szeptycka[52], T.Szumlak[19], T.Tabarelli[29], A.C.Taffard[23], F.Tegenfeldt[49], J.Timmermans[31], L.Tkatchev[16], M.Tobin[23], S.Todorovova[12], B.Tome[22], A.Tonazzo[29], P.Tortosa[50], P.Travnicek[12], D.Treille[8], G.Tristram[7], M.Trochimczuk[52], C.Troncon[28], M-L.Turluer[40], I.A.Tyapkin[16], P.Tyapkin[16], S.Tzamarias[11], V.Uvarov[42], G.Valenti[5], P.Van Dam[31], J.Van Eldik[8], N.van Remortel[15], I.Van Vulpen[8], G.Vegni[28], F.Veloso[22], W.Venus[37], P.Verdier[27], V.Verzi[38], D.Vilanova[40], L.Vitale[47], V.Vrba[12], H.Wahlen[53], C.Walck[44], A.J.Washbrook[23], C.Weiser[17], D.Wicke[8], J.Wickens[2], G.Wilkinson[35], M.Winter[9], M.Witek[18], O.Yushchenko[42], A.Zalewska[18], P.Zalewski[52], D.Zavrtanik[43], V.Zhuravlov[16], N.I.Zimin[16], A.Zintchenko[16], M.Zupan[11]

[1] Department of Physics and Astronomy, Iowa State University, Ames IA 50011-3160, USA
[2] Physics Department, Universiteit Antwerpen, Universiteitsplein 1, B-2610 Antwerpen, Belgium
and IIHE, ULB-VUB, Pleinlaan 2, B-1050 Brussels, Belgium
and Faculté des Sciences, Univ. de l'Etat Mons, Av. Maistriau 19, B-7000 Mons, Belgium
[3] Physics Laboratory, University of Athens, Solonos Str. 104, GR-10680 Athens, Greece
[4] Department of Physics, University of Bergen, Allégaten 55, NO-5007 Bergen, Norway
[5] Dipartimento di Fisica, Università di Bologna and INFN, Via Irnerio 46, IT-40126 Bologna, Italy
[6] Centro Brasileiro de Pesquisas Físicas, rua Xavier Sigaud 150, BR-22290 Rio de Janeiro, Brazil
and Depto. de Física, Pont. Univ. Católica, C.P. 38071 BR-22453 Rio de Janeiro, Brazil
and Inst. de Física, Univ. Estadual do Rio de Janeiro, rua São Francisco Xavier 524, Rio de Janeiro, Brazil
[7] Collège de France, Lab. de Physique Corpusculaire, IN2P3-CNRS, FR-75231 Paris Cedex 05, France
[8] CERN, CH-1211 Geneva 23, Switzerland
[9] Institut de Recherches Subatomiques, IN2P3 - CNRS/ULP - BP20, FR-67037 Strasbourg Cedex, France
[10] Now at DESY-Zeuthen, Platanenallee 6, D-15735 Zeuthen, Germany
[11] Institute of Nuclear Physics, N.C.S.R. Demokritos, P.O. Box 60228, GR-15310 Athens, Greece
[12] FZU, Inst. of Phys. of the C.A.S. High Energy Physics Division, Na Slovance 2, CZ-180 40, Praha 8, Czech Republic
[13] Dipartimento di Fisica, Università di Genova and INFN, Via Dodecaneso 33, IT-16146 Genova, Italy
[14] Institut des Sciences Nucléaires, IN2P3-CNRS, Université de Grenoble 1, FR-38026 Grenoble Cedex, France
[15] Helsinki Institute of Physics and Department of Physical Sciences, P.O. Box 64, FIN-00014 University of Helsinki, Finland
[16] Joint Institute for Nuclear Research, Dubna, Head Post Office, P.O. Box 79, RU-101 000 Moscow, Russian Federation
[17] Institut für Experimentelle Kernphysik, Universität Karlsruhe, Postfach 6980, DE-76128 Karlsruhe, Germany
[18] Institute of Nuclear Physics PAN,Ul. Radzikowskiego 152, PL-31142 Krakow, Poland
[19] Faculty of Physics and Nuclear Techniques, University of Mining and Metallurgy, PL-30055 Krakow, Poland
[20] Université de Paris-Sud, Lab. de l'Accélérateur Linéaire, IN2P3-CNRS, Bât. 200, FR-91405 Orsay Cedex, France
[21] School of Physics and Chemistry, University of Lancaster, Lancaster LA1 4YB, UK
[22] LIP, IST, FCUL - Av. Elias Garcia, 14-1°, PT-1000 Lisboa Codex, Portugal
[23] Department of Physics, University of Liverpool, P.O. Box 147, Liverpool L69 3BX, UK
[24] Dept. of Physics and Astronomy, Kelvin Building, University of Glasgow, Glasgow G12 8QQ
[25] LPNHE, IN2P3-CNRS, Univ. Paris VI et VII, Tour 33 (RdC), 4 place Jussieu, FR-75252 Paris Cedex 05, France
[26] Department of Physics, University of Lund, Sölvegatan 14, SE-223 63 Lund, Sweden
[27] Université Claude Bernard de Lyon, IPNL, IN2P3-CNRS, FR-69622 Villeurbanne Cedex, France
[28] Dipartimento di Fisica, Università di Milano and INFN-MILANO, Via Celoria 16, IT-20133 Milan, Italy
[29] Dipartimento di Fisica, Univ. di Milano-Bicocca and INFN-MILANO, Piazza della Scienza 2, IT-20126 Milan, Italy
[30] IPNP of MFF, Charles Univ., Areal MFF, V Holesovickach 2, CZ-180 00, Praha 8, Czech Republic
[31] NIKHEF, Postbus 41882, NL-1009 DB Amsterdam, The Netherlands
[32] National Technical University, Physics Department, Zografou Campus, GR-15773 Athens, Greece
[33] Physics Department, University of Oslo, Blindern, NO-0316 Oslo, Norway
[34] Dpto. Fisica, Univ. Oviedo, Avda. Calvo Sotelo s/n, ES-33007 Oviedo, Spain
[35] Department of Physics, University of Oxford, Keble Road, Oxford OX1 3RH, UK
[36] Dipartimento di Fisica, Università di Padova and INFN, Via Marzolo 8, IT-35131 Padua, Italy
[37] Rutherford Appleton Laboratory, Chilton, Didcot OX11 OQX, UK
[38] Dipartimento di Fisica, Università di Roma II and INFN, Tor Vergata, IT-00173 Rome, Italy
[39] Dipartimento di Fisica, Università di Roma III and INFN, Via della Vasca Navale 84, IT-00146 Rome, Italy
[40] DAPNIA/Service de Physique des Particules, CEA-Saclay, FR-91191 Gif-sur-Yvette Cedex, France
[41] Instituto de Fisica de Cantabria (CSIC-UC), Avda. los Castros s/n, ES-39006 Santander, Spain
[42] Inst. for High Energy Physics, Serpukov P.O. Box 35, Protvino, (Moscow Region), Russian Federation
[43] J. Stefan Institute, Jamova 39, SI-1000 Ljubljana, Slovenia and Laboratory for Astroparticle Physics,
University of Nova Gorica, Kostanjeviska 16a, SI-5000 Nova Gorica, Slovenia,
and Department of Physics, University of Ljubljana, SI-1000 Ljubljana, Slovenia
[44] Fysikum, Stockholm University, Box 6730, SE-113 85 Stockholm, Sweden
[45] Dipartimento di Fisica Sperimentale, Università di Torino and INFN, Via P. Giuria 1, IT-10125 Turin, Italy
[46] INFN,Sezione di Torino and Dipartimento di Fisica Teorica, Università di Torino, Via Giuria 1, IT-10125 Turin, Italy
[47] Dipartimento di Fisica, Università di Trieste and INFN, Via A. Valerio 2, IT-34127 Trieste, Italy
and Istituto di Fisica, Università di Udine, IT-33100 Udine, Italy
[48] Univ. Federal do Rio de Janeiro, C.P. 68528 Cidade Univ., Ilha do Fundão BR-21945-970 Rio de Janeiro, Brazil
[49] Department of Radiation Sciences, University of Uppsala, P.O. Box 535, SE-751 21 Uppsala, Sweden
[50] IFIC, Valencia-CSIC, and D.F.A.M.N., U. de Valencia, Avda. Dr. Moliner 50, ES-46100 Burjassot (Valencia), Spain
[51] Institut für Hochenergiephysik, Österr. Akad. d. Wissensch., Nikolsdorfergasse 18, AT-1050 Vienna, Austria
[52] Inst. Nuclear Studies and University of Warsaw, Ul. Hoza 69, PL-00681 Warsaw, Poland
[53] Fachbereich Physik, University of Wuppertal, Postfach 100 127, DE-42097 Wuppertal, Germany
† deceased

1 Introduction

This paper presents measurements of the masses and mean lifetimes of Ξ^- and $\overline{\Xi}^+$ and of their mass and lifetime differences, together with a study of $\Xi^{-\dagger}$ production in Z^0 hadronic decays.

Previous measurements of the $\overline{\Xi}^+$ mass and mean lifetime suffer from low statistics compared to Ξ^- measurements, since they came from bubble chamber or hyperon beam experiments with a large asymmetry in the production of Ξ^- and $\overline{\Xi}^+$. The Particle Data Group [1] lists only ~ 80 events used for measurement of the $\overline{\Xi}^+$ mass and 34 for its mean lifetime, compared to ~ 2400 events for the Ξ^- mass and ~ 87000 for its mean lifetime. The present analysis uses about 2500 Ξ^- and 2300 $\overline{\Xi}^+$, with small backgrounds. The symmetry in the production of particles and antiparticles in Z^0 decays makes direct measurements of Ξ^- and $\overline{\Xi}^+$ mass and lifetime differences with high precision feasible. A non-zero value of either difference would signal violation of CPT invariance.

A comparison of the Ξ production rates in $Z^0 \to b\bar{b}$ and $Z^0 \to q\bar{q}$ events is also presented, together with a measurement of the position ξ^* of the maximum of the distribution in $\xi = -\ln x_p$, where x_p is the fractional Ξ momentum.

2 The DELPHI detector and event selection

The DELPHI detector is described elsewhere [2,3]. The detectors most important for this analysis are the Vertex Detector (VD), the Inner Detector (ID), the Time Projection Chamber (TPC), and the Outer Detector (OD). The VD consists of three concentric layers of silicon strip detectors, located at radii of 6 cm, 9 cm and 11 cm. The data used here were taken in 1992-1995 inclusive, when the polar angles covered for particles crossing all three VD layers were $43° < \theta < 137°$, where θ is given with respect to the z axis[‡]. In 1994 and 1995, the first and third layers had double-sided readout and gave both $R\phi$ and z coordinates. The TPC is the main tracking device where charged-particle tracks are reconstructed in three dimensions for radii between 29 cm and 122 cm. The ID and OD are two drift chambers located at radii between 12 cm and 28 cm and between 198 cm and 206 cm respectively, and provide additional points for the track reconstruction.

A charged particle was accepted in the analysis if its track length was above 30 cm, its momentum above 100 MeV/c, and its relative momentum error below 100%.

An event was classified as hadronic if it had at least 7 charged particles with momentum above 200 MeV/c carrying more than 15 GeV reconstructed energy in total and at least 3 GeV in each hemisphere defined with respect to the z axis.

The analysis used 3.25 million reconstructed hadronic decays of the Z, consisting of 0.67 million from the 1992 run, 0.68 million from 1993, 1.29 million from 1994, and 0.61 million from 1995.

Simulated events were produced using the JETSET parton shower generator [4], and then processed with the DELPHI event simulation program DELSIM [3] which fully simulates all detector effects. For each of the years 1992 to 1994, about 1 million fully simulated $q\bar{q}$ events were analyzed in the same way as the real data, and about 0.6 million for 1995. The total number of simulated events used was thus about 3.6 million,

[†] Antiparticles are implicitly included unless explicitly stated otherwise.

[‡] In the standard DELPHI coordinate system, the z axis is along the electron direction, the x axis points towards the centre of LEP, and the y axis points upwards. The polar angle to the z axis is called θ and the azimuthal angle around the z axis is called ϕ; the radial coordinate is $R = \sqrt{x^2 + y^2}$.

comparable to the number of real events. The number of Ξ^- and $\overline{\Xi}^+$ decays generated in the simulation was about 89000.

3 Analysis

The Ξ^- hyperon was studied by a complete reconstruction of the decay chain $\Xi^- \to \Lambda\pi^-$, where $\Lambda \to p\pi^-$. A similar analysis procedure was used previously for Ω^- reconstruction [5].

All pairs of oppositely-charged particles were tried in a search for Λ candidates. For each such pair, a vertex fit was performed by the standard DELPHI V^0 search algorithm[§] [3]. A pair was accepted as a Λ candidate if the χ^2-probability of the secondary vertex fit exceeded 0.1%, the measured flight distance from the primary vertex of the Λ candidate in the xy plane exceeded twice its error, and the angle between the momentum vector sum of the two tracks and the vector joining the primary and secondary vertices was less than 0.1 radians (the loss of signal due to this cut has been shown to be negligible). The inclusive Λ reconstruction efficiency was around 19% [3], including the 63.9% branching ratio of $\Lambda \to \mathrm{p}\pi^-$ [1]. The invariant mass of the Λ candidate was required to be between 1.105 GeV/c^2 and 1.125 GeV/c^2.

One by one, the remaining tracks of charged particles that crossed the Λ trajectory in the xy plane were then combined with the Λ candidate to form a Ξ^- candidate. All Ξ^- were assumed to originate from the beam interaction point, which was calculated event by event.

A constrained fit was performed if:

- the intersection between the Λ and the charged particle trajectory was more than 8 mm away from the main vertex in the xy plane;
- the Λ and charged particle trajectories were less than 7 mm apart in the z direction at the point of crossing in the xy plane;
- and the charged particle had an impact parameter with respect to the main vertex in the xy plane of at least 0.5 mm.

The fit used was a general least squares fit with kinematical and geometrical constraints applied to each Ξ^- candidate. The 16 measured variables in the fit were the five parameters of the helix parameterization of each of the three charged particle tracks and the z coordinate of the beam interaction point (the x and y coordinates were so precisely measured that they could be taken as fixed). The two unmeasured variables were the decay radii of the Ξ^- and Λ. The Ξ^- decay point was then determined from this Ξ^- decay radius and the π^- trajectory while the Λ decay point was determined from the point on the proton trajectory at the Λ decay radius. The curved Ξ^- track was not measured, but calculated in the fit.

Four constraints required the momenta of the Ξ^- and Λ at their decay points to be in the same direction as the trajectory joining their production and decay positions, two required the other π^- to meet the proton at the Λ decay radius, and the last (seventh) constrained the Λ mass to its nominal value (1115.684$\pm$0.006) MeV/c^2. For further details concerning the fitting procedure, see [6].

The pull distributions of the 16 fitted quantities were all approximately normally distributed, with mean 0 within $\pm$0.1 and standard deviation 1 within $\pm$0.1, both for data and for the simulated events.

The following cuts were used to select the Ξ^- and $\overline{\Xi}^+$ samples:

[§] A V^0 consists of two oppositely charged particles originating from a neutral particle decaying in flight.

Year	92	93	94	95
M_{Ξ^-} in data	1321.60 ± 0.17	1321.25 ± 0.16	1321.45 ± 0.10	1321.50 ± 0.16
M_{Ξ^+} in data	1321.70 ± 0.18	1321.49 ± 0.14	1321.46 ± 0.12	1321.19 ± 0.18
$M_{\Xi^\pm}$ in data	1321.65 ± 0.13	1321.37 ± 0.11	1321.45 ± 0.08	1321.36 ± 0.12
$M_{\Xi^-} - M_{\Xi^+}$ in data	-0.10 ± 0.25	-0.23 ± 0.22	-0.02 ± 0.15	0.31 ± 0.24
$M_{\Xi^\pm} - 1321.3$ in MC	0.14 ± 0.07	-0.02 ± 0.07	0.06 ± 0.07	0.30 ± 0.09
Corrected M_{Ξ^-}:	1321.46 ± 0.18	1321.27 ± 0.17	1321.39 ± 0.12	1321.20 ± 0.19
Corrected M_{Ξ^+}:	1321.56 ± 0.19	1321.51 ± 0.16	1321.40 ± 0.14	1320.89 ± 0.20
Corrected $M_{\Xi^\pm}$:	1321.51 ± 0.15	1321.39 ± 0.12	1321.39 ± 0.10	1321.06 ± 0.15

Table 1: Ξ^- and $\overline{\Xi}^+$ mass fit results. Values are in MeV/c^2. In the simulated ('MC') sample, the generated Ξ^- mass was 1321.3 MeV/c; the corresponding mass shifts per year are used to correct the mass values found in the data. The errors are statistical only.

- the χ^2-probability of the fit had to exceed 1%;
- the Ξ momentum, p_Ξ, had to fulfill $1.2 < \xi < 4.2$ where $\xi = -\ln x_p$ and $x_p = p_\Xi / p_{beam}$; this corresponds to $0.015 < x_p < 0.3$ or $0.7 < p_\Xi < 14$ GeV/c;
- the Ξ momentum had to point into the barrel region of the detector ($|\cos\theta| < 0.85$);
- the decay radius of the Ξ in the xy plane had to exceed 2 cm;
- the decay radius of the Ξ in the xy plane had to be less than the Λ decay radius.

Figure 1 shows the right-sign ($\Lambda\pi^-$ and $\overline{\Lambda}\pi^+$) mass distributions and the Ξ signals before and after the cuts were applied. Apart from a difference in mass resolution, the agreement between data and simulation was very good. The distributions of the variables used in the selection of Ξ candidates are shown in Figure 2 for wrong-sign ($\Lambda\pi^+$ and $\overline{\Lambda}\pi^-$) as well as for right-sign ($\Lambda\pi^-$ and $\overline{\Lambda}\pi^+$) combinations.

The fit gave a narrow mass peak from Ξ decays on a small background, as shown in Figure 3a; 2478 ± 68 Ξ^- and 2256 ± 63 $\overline{\Xi}^+$ decays were reconstructed, as shown in Figures 3b and 3c. The fitted curves consist of a linear term for the background, and two Gaussian distributions with common mean for the signal. The Ξ mass resolution depends on momentum. Therefore the signal is, in principle, the sum of an infinite number of Gaussians. But two give a reasonably good fit. The fitted widths of the two Gaussians were (2.0 ± 0.1) MeV/c^2 and (5.6 ± 0.4) MeV/c^2, with a relative fraction of 1.29 ± 0.18. The corresponding widths from fitting simulated data were (1.8 ± 0.1) MeV/c^2 and (5.5 ± 0.5) MeV/c^2, with a relative fraction of 2.01 ± 0.27. This parameterization of signal and background was used in the determination of the Ξ^- and $\overline{\Xi}^+$ masses.

The only possible physical background is the decay $\Omega^\pm \to \Lambda K^\pm$. The number of Ω^- reconstructed in our Ξ^-analysis is estimated to be at most five, and consequently to have no significant influence.

3.1 Measurement of Ξ^- and $\overline{\Xi}^+$ masses and mass difference

Table 1 gives the fitted mass and mass difference values for the real data. As already described, the signal (see Figure 3) was represented by two Gaussian distributions with common mean and the background by a linear term.

Year	92	93	94	95
M_{K^0} offset in data	-0.87 ± 0.06	-1.09 ± 0.05	-0.75 ± 0.06	-0.80 ± 0.06
M_{K^0} offset in MC	0.01 ± 0.05	0.56 ± 0.04	0.38 ± 0.04	0.68 ± 0.04
Corrected M_{K^0} offset	-0.88 ± 0.09	-1.65 ± 0.08	-1.13 ± 0.09	-1.48 ± 0.09
M_Λ offset in data	0.14 ± 0.05	-0.14 ± 0.05	-0.09 ± 0.06	-0.07 ± 0.06
M_Λ offset in MC	0.09 ± 0.06	0.01 ± 0.04	0.09 ± 0.04	0.17 ± 0.04
Corrected M_Λ offset	0.04 ± 0.08	-0.15 ± 0.07	-0.18 ± 0.08	-0.24 ± 0.08
Calculated M_Ξ offset	-0.13 ± 0.09	-0.44 ± 0.07	-0.36 ± 0.06	-0.47 ± 0.07
Resulting $M_{\Xi^\pm}$	1321.64 ± 0.17	1321.82 ± 0.14	1321.75 ± 0.12	1321.53 ± 0.17

Table 2: Measured offsets from the nominal K^0 and Λ masses in MeV/c^2, and the corresponding offsets in Ξ mass, together with the final, resulting $\Xi^\pm$ mass values. The errors of the corrected K^0 and Λ masses include the spread from the simulation smearing, see text.

In order to correct for any bias due to the data processing or to the analysis and fit procedure, the mass values obtained from the data were corrected by the difference between the values obtained in the same way from the simulated events and the input value used in the simulation (1321.3 MeV/c^2). As no effect could be identified that might affect the $\Xi^-$and $\overline{\Xi}^+$masses differently, the correction was calculated once for each year, using the corresponding fully simulated $\Xi^\pm$ sample. Table 1 also shows these corrections, and the corrected mass values. The statistical errors of the corrected values contain the statistical errors of the simulation.

The $\Xi^\pm$ mass value averaged over all years was (1321.45 ± 0.05) MeV/c^2 with a χ^2 probability for the combination of 33% before correction, and (1321.35 ± 0.06) MeV/c^2 with a χ^2 probability of 17% after correction. Thus the average correction amounted to (-0.10 ± 0.04) MeV/c^2.

3.1.1 Mass scale calibration

The mass scale was calibrated by determining the Λ and K^0_s masses in the same way, and comparing the resulting values with the known values [1]. The Λ and K^0_s samples used for this purpose were spread over each whole year and their sizes were restricted to make it possible to use the same signal and background parameterizations as for the Ξ[¶].

The Λ and K^0_s decays were reconstructed by considering all pairs of oppositely charged particles, and the vertex defined by each pair was determined by minimizing the χ^2 of the extrapolated tracks. Consequently, this was a purely geometrical vertex fit, as opposed to the mass-constrained fit described above for the Ξ candidates. The measured Λ and K^0_s mass offsets from their nominal values are shown in Table 2.

The widths of the Λ and K^0_s mass distributions are somewhat larger for data than for simulation. A study was made in which the reconstructed variables in simulation, one by one, were artificially "smeared" and a corresponding extra measurement error added, such that the width of the mass peak in simulation agreed with that in the data. The spreads of the shifts obtained by smearing different variables, amounting to 0.05 MeV/c^2

[¶]The reconstructed Λ samples were typically twice as large as the reconstructed Ξ samples while the K^0_s samples were typically 10 times larger

for K^0 and 0.04 MeV/c^2 for Λ, were included in the errors for the corrected offsets quoted in Table 2. However, the means of the mass values from the smearings agreed with the "unsmeared" values.

Offsets of the corrected Λ and K^0_s mass values from their known values can arise from an error in the correction for dE/dx losses, an error in the assumed magnetic field, or, most likely, a combination of the two.

The Ξ mass offset can be expressed as a function of the K^0_s and Λ mass offsets, as

$$\Delta M_\Xi = (b_\Xi \quad d_\Xi) \begin{pmatrix} b_K & d_K \\ b_\Lambda & d_\Lambda \end{pmatrix}^{-1} \begin{pmatrix} \Delta M_K \\ \Delta M_\Lambda \end{pmatrix}$$

where b_i are the Ξ, K^0_s and Λ mass shift coefficients due to magnetic field changes, and d_i are those due to dE/dx correction changes. The values of these coefficients were found using Monte Carlo techniques: $b_\Xi = 0.0805 \pm 0.0004$, $b_K = 0.2376 \pm 0.0010$, $b_\Lambda = 0.0438 \pm 0.0002$, $d_\Xi = 0.20 \pm 0.02$, $d_K = 0.367 \pm 0.017$ and $d_\Lambda = 0.162 \pm 0.011$.

Inserting the observed K^0_s and Λ mass shifts and the mass offset coefficients into the above equation, taking all errors into account, gave the Ξ mass offsets presented in Table 2. The last line of that table gives the final corrected $\Xi^\pm$ mass values per year. The final average corrected mass value is $(1321.71 \pm 0.06 \pm 0.04)$ MeV/c^2 with a χ^2 probability for the combination of 53%. The second error quoted is the unfolded contribution from the uncertainty in the calibration offsets.

3.1.2 Other systematic uncertainties

The effect of using different parameterizations for the shape of the Ξ mass peak and for the background was studied, as well as that of using various fitting techniques (maximum likelihood and minimum χ^2). These variations gave a spread in the final Ξ mass value of ± 0.03 MeV/c^2.

Applying the same "smearing" technique to the simulated Ξ events as was described above for the Λ and K^0_s analysis gave a spread in the final Ξ mass value of ± 0.02 MeV/c^2. Again the average of the values from the smearing study agreed with the unsmeared value.

As a cross-check, the Ξ mass was measured as a function of the momentum of the pion from the Ξ^- decay. This is generally the one passing through the most material, and it is not affected by the Λ mass constraint. Thus it is the one most sensitive to dE/dx corrections. No systematic effect depending on the pion momentum was observed. The Ξ mass was also measured as a function of the polar angle of the Ξ momentum and of the observed distance in the xy plane from the beam axis. Again no systematic variation was found.

The total systematic error was thus ± 0.05 MeV/c^2, as shown in Table 3.

3.1.3 Results

The measured average Ξ masses are:

$$\begin{aligned} M_{\Xi^-} &= (1321.70 \pm 0.08 \text{ (stat.)} \pm 0.05 \text{ (syst.)}) \text{ MeV}/c^2 \\ M_{\Xi^+} &= (1321.73 \pm 0.08 \text{ (stat.)} \pm 0.05 \text{ (syst.)}) \text{ MeV}/c^2 \\ M_{\Xi^-+\Xi^+} &= (1321.71 \pm 0.06 \text{ (stat.)} \pm 0.05 \text{ (syst.)}) \text{ MeV}/c^2, \end{aligned}$$

where the systematic errors quoted are common to all three values.

Source	MeV/c^2
Λ and K^0 mass scale	± 0.04
Fit parameterization	± 0.03
Simulation smearing	± 0.02
total	± 0.05

Table 3: Systematic error contributions to the Ξ mass measurement.

The systematic errors cancel in the mass difference[‖], where the small statistical errors on the uncorrected values can therefore be fully exploited. The mass difference measured in the data is

$$\Delta_{\rm M} = {\rm M}_{\Xi^-} - {\rm M}_{\Xi^+} = (-0.03 \pm 0.12)\ {\rm MeV/c^2}$$

which corresponds to a fractional mass difference of

$$({\rm M}_{\Xi^-} - {\rm M}_{\Xi^+})/{\rm M}_{average} = (-2.5 \pm 8.7) \times 10^{-5}.$$

This improves the precision on this CPT violation test quantity by a factor of 3 compared to the current PDG value of $(11 \pm 27) \times 10^{-5}$ [1].

3.2 Measurement of Ξ^- and $\overline{\Xi}^+$ lifetimes and lifetime difference

The measurement of the mean lifetimes of the Ξ^- and $\overline{\Xi}^+$ and their lifetime differences uses the Ξ^- and $\overline{\Xi}^+$ candidates with a $\Lambda\pi$ invariant mass within ± 5 MeV/c^2 of the nominal mass, where the signal to background ratio is about 6:1. This is the sample for which data and simulation were compared in detail in Figure 2.

The mean lifetimes were estimated using a maximum likelihood fit. The time distribution of the combinatorial background was estimated simultaneously in the fit by using the wrong-sign combinations. The observed proper time distributions and the fitted functions for the wrong-sign and right-sign distributions are shown in Figures 4 and 5 respectively. As the mean lifetimes are much shorter for c- and b-baryons than for a Ξ, all Ξ may safely be assumed to originate from the interaction point.

The proper time was calculated as

$$t \;=\; d_\Xi M_\Xi / P_\Xi \tag{1}$$

where d_Ξ is the fitted flight distance in the xy plane, P_Ξ is the fitted momentum of the Ξ candidate in the xy plane, and M_Ξ is the nominal Ξ mass.

For right-sign and wrong-sign candidates in the proper time interval 0.04 ns to 2.0 ns, the following likelihood function was formed:

$$\mathcal{L} \;=\; \prod_{i=1}^{N_{rs}} F(t_i) \;\cdot \prod_{j=1}^{N_{ws}} B(t_j). \tag{2}$$

The first factor, the $F(t)$ product, represents the right-sign ($\Lambda\pi^-$, $\overline{\Lambda}\pi^+$) combinations. The second factor, the $B(t)$ product, is an empirical parameterization of the wrong-sign ($\Lambda\pi^+$, $\overline{\Lambda}\pi^-$) combinations. The same function $B(t)$ was also used to describe the

[‖] It was checked that there was no difference between masses of Λ and $\overline{\Lambda}$, and that the K^0 mass did not depend on the charge of the highest momentum particle in the decay.

Year	92	93	94	95
τ_{Ξ^-}	0.131 ± 0.012	0.179 ± 0.014	0.199 ± 0.015	0.167 ± 0.016
τ_{Ξ^+}	0.165 ± 0.015	0.146 ± 0.013	0.205 ± 0.015	0.169 ± 0.020
$\Delta\tau = \tau_{\Xi^-} - \tau_{\Xi^+}$	-0.034 ± 0.020	$+0.033 \pm 0.019$	-0.006 ± 0.021	-0.002 ± 0.025

Table 4: Fit results and statistical errors for Ξ^- and $\overline{\Xi}^+$ lifetime fits. Values are in nanoseconds.

background in the right-sign sample. Thus, by maximizing the joint likelihood function $\mathcal{L}$, the background contribution in the right-sign sample was naturally constrained to the shape of the wrong-sign distribution.

The right-sign function $F(t)$ was given by

$$F(t) = \frac{1}{\sigma_0 + 1}\left(\sigma_0 S(t) + B(t)\right) \tag{3}$$

where $S(t)$ is a normalized probability density function for the observed signal, *i.e.* it is proportional to $\epsilon(t)e^{-t/\tau_\Xi}$, where $\epsilon(t)$ is an empirical efficiency parameterization of the time-dependent form $e^{(c_1+c_2 t)}$ determined from the simulation. The relative normalization of the signal $S(t)$ and background $B(t)$ in the right-sign sample, σ_0, was fixed by the observed number of right-sign (N_{rs}) and wrong-sign (N_{ws}) events in the fitted time interval 0.04 ns to 2.0 ns, $\sigma_0 = \frac{N_{rs}-N_{ws}}{N_{ws}}$.

The background function $B(t)$ was given by

$$B(t) = \frac{1}{b_1 + 1}\left\{b_1 \frac{b(t;\sigma_1)}{\mathcal{N}_1} + \frac{b(t;\sigma_2)}{\mathcal{N}_2}\right\} \tag{4}$$

where

$$b(t;\sigma_i) = \frac{1}{\Gamma(\beta)\sigma_i}\left(\frac{t}{\sigma_i}\right)^{\beta-1} e^{-\frac{t}{\sigma_i}}. \tag{5}$$

and $\mathcal{N}_1$ and $\mathcal{N}_2$ are normalization constants for the two Γ-distributions $b(t;\sigma_i)$. The value $\beta = 3$ provided a good description of the wrong-sign distribution. The parameters b_1, σ_1 and σ_2 were fitted to the data, together with τ_Ξ. The fit results for each year are given in Table 4.

The measured Ξ^- and $\overline{\Xi}^+$ lifetimes are:

$$\begin{aligned}
\tau_{\Xi^-} &= (0.165 \pm 0.007\ (\text{stat.})\ \pm 0.012\ (\text{syst.}))\ \text{ns} \\
\tau_{\Xi^+} &= (0.170 \pm 0.008\ (\text{stat.})\ \pm 0.012\ (\text{syst.}))\ \text{ns} \\
\tau_{\Xi^- + \Xi^+} &= (0.167 \pm 0.006\ (\text{stat.})\ \pm 0.012\ (\text{syst.}))\ \text{ns}
\end{aligned}$$

where the results were achieved by performing the same analysis on the four separate years. The lifetimes were taken as the weighted average of the four years.

In order to minimize the effect of statistical fluctuations, the combined Ξ^- and $\overline{\Xi}^+$ sample was used to evaluate the systematic errors. The following sources of systematic errors were considered:

- the effect on the lifetime fits of the uncertainty in the parameters c_1 and c_2 in the efficiency parameterization was estimated using the simulation to be ± 0.005 ns;

- the difference between the input and reconstructed lifetimes in the simulation was (0.002±0.004) ns;
- changing the fit range between 0.04 ns and 0.08 ns for the lower boundary and between 0.6 ns and 2.0 ns for the upper boundary changed the fitted lifetime by ±0.004 ns;
- changing the value of β (Equation 5) in the range 1.5 to 4.0 had no significant influence on the final results;
- the χ^2 of the combination of the four different years was 14.1 for 3 degrees of freedom corresponding to a probability of only 0.3%; applying the PDG scaling procedure to the combination gives an additional systematic error of ±0.011 ns.

Note that a Ξ could be reconstructed only if the (anti)proton from the (anti)lambda was seen in the TPC. Therefore the fact that more antibaryons than baryons interacted in the material before the TPC reduced the relative number of $\overline{\Xi}^+$ reconstructed by about 10%, but had no significant effect on their lifetime distribution. Thus the systematic errors quoted above are common to all three lifetime values.

The systematic errors cancel in the measurement of the lifetime difference, averaged over the years:

$$< \Delta\tau >=< \tau_{\Xi^-} - \tau_{\Xi^+} >= (-0.002 \pm 0.011) \text{ ns},$$

which gives a fractional lifetime difference of

$$(\tau_{\Xi^-} - \tau_{\Xi^+})/\tau_{average} = -0.01 \pm 0.07.$$

This quantity, which would indicate violation of CPT invariance if different from zero, has a much smaller error than the PDG value of 0.02 ± 0.18 [1].

The value of $\Delta\tau$ may also be used together with the world average for the Ξ^- lifetime, $\tau_{\Xi^-}^{\rm PDG} = (0.1639 \pm 0.0015)$ ns, to make a new precise determination of the $\overline{\Xi}^+$ lifetime alone:

$$\tau_{\Xi^+} = \tau_{\Xi^-}^{\rm PDG} - \Delta\tau = (0.166 \pm 0.011) \text{ ns}.$$

3.3 Measurements of Ξ^- and $\overline{\Xi}^+$ production

The parameterization of the signal used in the Ξ mass determination was not used to evaluate the efficiencies and production rates, since the broader Gaussian tended to become unreasonably wide if left free when fitting substantially smaller data samples. Instead, as in the lifetime analysis just described, a fixed interval, this time ±10 MeV/c^2 around the nominal Ξ^- mass, was used as signal region. The background was estimated from the wrong-sign invariant mass distributions.

The efficiency was determined from simulation and depended on the Ξ momentum (see Table 5 and Figure 6). The average efficiency was found to be (6.76 ± 0.27 (stat.))% for the combined Ξ^- and $\overline{\Xi}^+$ reconstruction, including cuts and the 63.9% branching ratio for $\Lambda \to {\rm p}\pi^-$. The error comes from the finite number of simulated events. As mentioned earlier, the reconstruction efficiency was $\sim 10\%$ lower for $\overline{\Xi}^+$ than for Ξ^-, due to differences in the cross-sections for hadronic interactions of particles and antiparticles in the detector material.

All Ξ^- candidates satisfying the standard Ξ^- cuts, and with a $\Lambda\pi^-$ invariant mass within ±10 MeV/c^2 of the nominal Ξ^- mass, were considered. The background contribution was estimated from the wrong-sign combinations and was subtracted. The measured distribution in $\xi = -\ln x_p$ is shown in Figure 6 and Table 5. The $< \Xi^- + \overline{\Xi}^+ >$ production rate in the ξ interval $1.4 < \xi < 4.0$ was found to be

$$< \Xi^- + \overline{\Xi}^+ >_{q\bar{q}} = 0.0197 \pm 0.0007 \text{ (stat.)}$$

where the statistical error includes the contributions from data and simulation. Extrapolating to the full momentum range using the JETSET prediction gave

$$< \Xi^- + \overline{\Xi}^+ >_{q\bar{q}} \ = 0.0247 \pm 0.0009 \text{ (stat.)} \ \pm 0.0025 \text{ (syst.)}$$

in hadronic Z decays. This result agrees with the previous DELPHI value of $0.0250 \pm 0.0009 \pm 0.0021$ [7], obtained using a somewhat different Ξ reconstruction procedure, and with the OPAL value of $0.0259 \pm 0.0004 \pm 0.0009$ [8]. For comparison, the DELPHI tuned JETSET 7.3 [9] gives 0.0251 and JETSET 7.4 with default parameters gives 0.0273, whereas HERWIG 5.9 [10] gives 0.0730.

The systematic error quoted above has the following two sources. Firstly, according to the simulation, 20% of the Ξ^- and $\overline{\Xi}^+$ were produced outside the range $1.4 < \xi < 4.0$. An error of 50% of this number was taken as a contribution to the total systematic error. Secondly, adding a cut on lifetime, $\tau_\Xi > 0.1$ ns, and requiring the Λ candidate to be tagged as a 'tight' Λ (xy flight distance above four standard deviations and χ^2 probability larger than 1%) by the V^0 reconstruction program gives a very clean sample. The production rate calculated with this sample, extrapolated to the full momentum range, is 0.0258 ± 0.0012(stat.), which is the same as that above within errors. The half-difference of the rates calculated with the two different sets of cuts was added in quadrature to give the total systematic error. The effect of varying the width of the signal region was very small.

From a Gaussian fit in the interval $1.4 < \xi < 4.0$, the ξ distribution was found to have a maximum at

$$\xi^*_{data} = 2.50 \pm 0.06 \text{ (stat.)} \ \pm 0.04 \text{ (syst.)}$$

where the systematic error was evaluated by varying the fit region and the Ξ mass window. The JETSET model, with parameters tuned as in [9], gave $\xi^*_{JETSET} = 2.522 \pm 0.004$(stat.) from a similar fit. These values are slightly lower than the OPAL measurement of $\xi^* = 2.72 \pm 0.13$ [8].

The large statistics of the JETSET Ξ^- sample clearly showed that the generated ξ distribution was not Gaussian. However, fitting a modified Gaussian form [11] to the generated ξ spectrum gave $\xi^* = 2.506 \pm 0.004$, very close to the result of fitting the unmodified Gaussian. Fitting the same modified form to the data, keeping the skewness and kurtosis parameters fixed to the values found in the simulation, gave $\xi^* = 2.51 \pm 0.06$(stat). These fits were also to the region $1.4 < \xi < 4.0$.

The above procedure for finding Ξ^- was also applied to $Z \to b\bar{b}$ decays. The $b\bar{b}$ events were selected with a lifetime tag algorithm [3,12]. This technique is based on the measurement of the impact parameter of each particle relative to the Z^0 production point. Decay products from particles with relatively long lifetimes, like B-hadrons, will have large impact parameters. Particles produced in the primary interaction will have impact parameters with a spread around zero according to the spatial resolution of the detector. From all tracks with a positive impact parameter in an event, the probability for the hypothesis that they all came from a single point was calculated. Events in which this probability was below 1% were selected as $b\bar{b}$ events. The joint efficiency to reconstruct a Ξ^- decay and simultaneously tag a $b\bar{b}$ event with this cut was about 3%, with a $b\bar{b}$ purity of 77%. Using these results the production rate of Ξ^- and $\overline{\Xi}^+$ in $b\bar{b}$ events was calculated. Taking the weighted average of the results from the four years gives the final rate:

$$< \Xi^- + \overline{\Xi}^+ >_{b\bar{b}} = 0.0183 \pm 0.0016 \text{ (stat.)} \ \pm 0.0035 \text{ (syst.)}$$

Momentum (GeV/c)	x_p	$\xi = -\ln x_p$	Efficiency (%)	Reconstructed Ξ^-	N_Ξ/bin/event
9.21–11.24	0.202–0.246	1.4–1.6	1.7±0.4	65±17	0.00118±0.00042
7.54–9.21	0.165–0.202	1.6–1.8	3.7±0.4	173±21	0.00145±0.00026
6.17–7.54	0.135–0.165	1.8–2.0	5.0±0.4	290±28	0.00178±0.00024
5.05–6.17	0.111–0.135	2.0–2.2	8.2±0.5	474±33	0.00177±0.00016
4.14–5.05	0.091–0.111	2.2–2.4	10.5±0.6	604±35	0.00180±0.00014
3.39–4.14	0.074–0.091	2.4–2.6	11.9±0.6	758±37	0.00196±0.00014
2.77–3.39	0.061–0.074	2.6–2.8	11.7±0.6	804±38	0.00210±0.00014
2.27–2.77	0.050–0.061	2.8–3.0	13.0±0.6	747±36	0.00176±0.00011
1.86–2.27	0.041–0.050	3.0–3.2	11.9±0.6	633±31	0.00165±0.00011
1.52–1.86	0.033–0.041	3.2–3.4	8.9±0.5	433±27	0.00151±0.00012
1.25–1.52	0.027–0.033	3.4–3.6	6.7±0.5	221±20	0.00101±0.00012
1.02–1.25	0.022–0.027	3.6–3.8	4.5±0.4	133±16	0.00092±0.00014
0.84–1.02	0.018–0.022	3.8–4.0	2.5±0.4	64±12	0.00081±0.00020

Table 5: Ξ^- efficiency and ξ distribution.

where the systematic error comes from the momentum extrapolation and the sample variation of the four years' data. Different cuts on the probability as well as looser Ξ^- selections were also tested. The value of $< \Xi^- + \overline{\Xi}^+ >_{b\bar{b}}$ changed only within ±0.001. The DELPHI tuned JETSET 7.3 [9] gives $< \Xi^- + \overline{\Xi}^+ >_{b\bar{b}}$ =0.0238 and JETSET 7.4 with default parameters gives 0.0208, whereas HERWIG 5.9 gives $< \Xi^- + \overline{\Xi}^+ >_{b\bar{b}} = 0.0523$.

4 Summary

About 2500 Ξ^- and 2300 $\overline{\Xi}^+$ decays have been reconstructed from data collected by the DELPHI detector in the years 1992 to 1995.

From this large sample, direct measurements have been made of the Ξ^- and $\overline{\Xi}^+$ masses and their average and difference:

$$\begin{aligned}
M_{\Xi^-} &= (1321.70 \pm 0.08\ (\text{stat.}) \pm 0.05\ (\text{syst.}))\ \text{MeV/c}^2 \\
M_{\Xi^+} &= (1321.73 \pm 0.08\ (\text{stat.}) \pm 0.05\ (\text{syst.}))\ \text{MeV/c}^2 \\
M_{\Xi^- + \Xi^+} &= (1321.71 \pm 0.06\ (\text{stat.}) \pm 0.05\ (\text{syst.}))\ \text{MeV/c}^2 \\
M_{\Xi^-} - M_{\Xi^+} &= (-0.03 \pm 0.12)\ \text{MeV/c}^2 \\
(M_{\Xi^-} - M_{\Xi^+})/M_{average} &= (-2.5 \pm 8.7) \times 10^{-5}.
\end{aligned}$$

The masses given by the PDG [1] are $M_{\Xi^-} = (1321.34 \pm 0.14)$ MeV/c^2, $M_{\Xi^+} = (1321.20 \pm 0.33)$ MeV/c^2 and $(M_{\Xi^-} - M_{\Xi^+}) / M_{average} = (11 \pm 27) \times 10^{-5}$. Up to now only small samples of $\overline{\Xi}^+$ are referenced by the PDG.

The Ξ^- lifetime measurement obtained is consistent with the PDG value of (0.1639 ± 0.0015) ns but has a much larger error. The lifetime difference obtained:

$$\Delta\tau = \tau_{\Xi^-} - \tau_{\Xi^+} = (-0.002 \pm 0.011)\ \text{ns}$$

implies

$$(\tau_{\Xi^-} - \tau_{\Xi^+})/\tau_{average} = -0.01 \pm 0.07$$

and, using the PDG value for τ_{Ξ^-},

$$\tau_{\Xi^+} = (0.166 \pm 0.011) \text{ ns},$$

which is more precise than our direct measurement, $\tau_{\Xi^+} = (0.170 \pm 0.008 \pm 0.012)$ ns. The present PDG values [1] for the fractional lifetime difference and for the $\overline{\Xi}^+$ lifetime are $(\tau_{\Xi^-} - \tau_{\Xi^+})/\tau_{average} = 0.02 \pm 0.18$ and $\tau_{\Xi^+} = (0.16 \pm 0.03)$ ns respectively.

Thus this analysis significantly improves the precision on the fractional mass and lifetime differences of Ξ^- and $\overline{\Xi}^+$, which test CPT invariance, compared to the present PDG values.

The inclusive production rates for Ξ^- plus $\overline{\Xi}^+$ in hadronic Z decays and in $Z \to b\bar{b}$ decays were found to be:

$$\begin{aligned} < \Xi^- + \overline{\Xi}^+ >_{q\bar{q}} &= 0.0247 \pm 0.0009 \text{ (stat.)} \pm 0.0025 \text{ (syst.)} \\ < \Xi^- + \overline{\Xi}^+ >_{b\bar{b}} &= 0.0183 \pm 0.0016 \text{ (stat.)} \pm 0.0035 \text{ (syst.)} \end{aligned}$$

The JETSET predictions agree with these measurements, whereas the HERWIG predictions do not. The maximum of the $\xi = -\ln x_p$ distribution was found to be at

$$\xi^* = 2.50 \pm 0.06 \text{ (stat.)} \pm 0.04 \text{ (syst.)}$$

in hadronic Z decays.

Acknowledgements

We are greatly indebted to our technical collaborators, to the members of the CERN-SL Division for the excellent performance of the LEP collider, and to the funding agencies for their support in building and operating the DELPHI detector.
We acknowledge in particular the support of
Austrian Federal Ministry of Education, Science and Culture, GZ 616.364/2-III/2a/98,
FNRS–FWO, Flanders Institute to encourage scientific and technological research in the industry (IWT), Belgium,
FINEP, CNPq, CAPES, FUJB and FAPERJ, Brazil,
Czech Ministry of Industry and Trade, GA CR 202/99/1362,
Commission of the European Communities (DG XII),
Direction des Sciences de la Matière, CEA, France,
Bundesministerium für Bildung, Wissenschaft, Forschung und Technologie, Germany,
General Secretariat for Research and Technology, Greece,
National Science Foundation (NWO) and Foundation for Research on Matter (FOM), The Netherlands,
Norwegian Research Council,
State Committee for Scientific Research, Poland, SPUB-M/CERN/PO3/DZ296/2000, SPUB-M/CERN/PO3/DZ297/2000, 2P03B 104 19 and 2P03B 69 23(2002-2004)
FCT - Fundação para a Ciência e Tecnologia, Portugal,
Vedecka grantova agentura MS SR, Slovakia, Nr. 95/5195/134,
Ministry of Science and Technology of the Republic of Slovenia,
CICYT, Spain, AEN99-0950 and AEN99-0761,
The Swedish Research Council,

Particle Physics and Astronomy Research Council, UK,
Department of Energy, USA, DE-FG02-01ER41155,
EEC RTN contract HPRN-CT-00292-2002.

References

[1] Particle Data Group, S. Eidelman et al., Phys. Lett. **B592** (2004) 1.
[2] DELPHI Collaboration, P. Aarnio et al., Nucl. Instr. and Meth. **A303** (1991) 233.
[3] DELPHI Collaboration, P. Abreu et al., Nucl. Instr. and Meth. **A378** (1996) 57.
[4] T. Sjöstrand, Comp. Phys. Comm. **82** (1994) 74.
[5] DELPHI Collaboration, W. Adam et al., Z. Phys. **C70** (1996) 371.
[6] "TULIP - a Constrained Fit Routine for Cascade Decays", P.Niss, M.Feindt, DELPHI note 96-149 TRACK 86,
http://delphiwww.cern.ch/pubxx/delnote/public/96_149_track_86.ps.gz .
[7] DELPHI Collaboration, P. Abreu et al., Z. Phys. **C67** (1995) 543.
[8] OPAL Collaboration, G. Alexander et al., Z. Phys. **C73** (1997) 569.
[9] DELPHI Collaboration, P. Abreu et al., Z. Phys. **C73** (1996) 11.
[10] G. Marchesini et al., Comp. Phys. Comm. **67** (1992) 465.
[11] Yu.L. Dokshitzer, V.A. Khoze and S.I. Troyan, Z. Phys. **C55** (1992) 107.
[12] G. Borisov and C. Mariotti, Nucl. Instr. and Meth. **A372** (1996) 181.

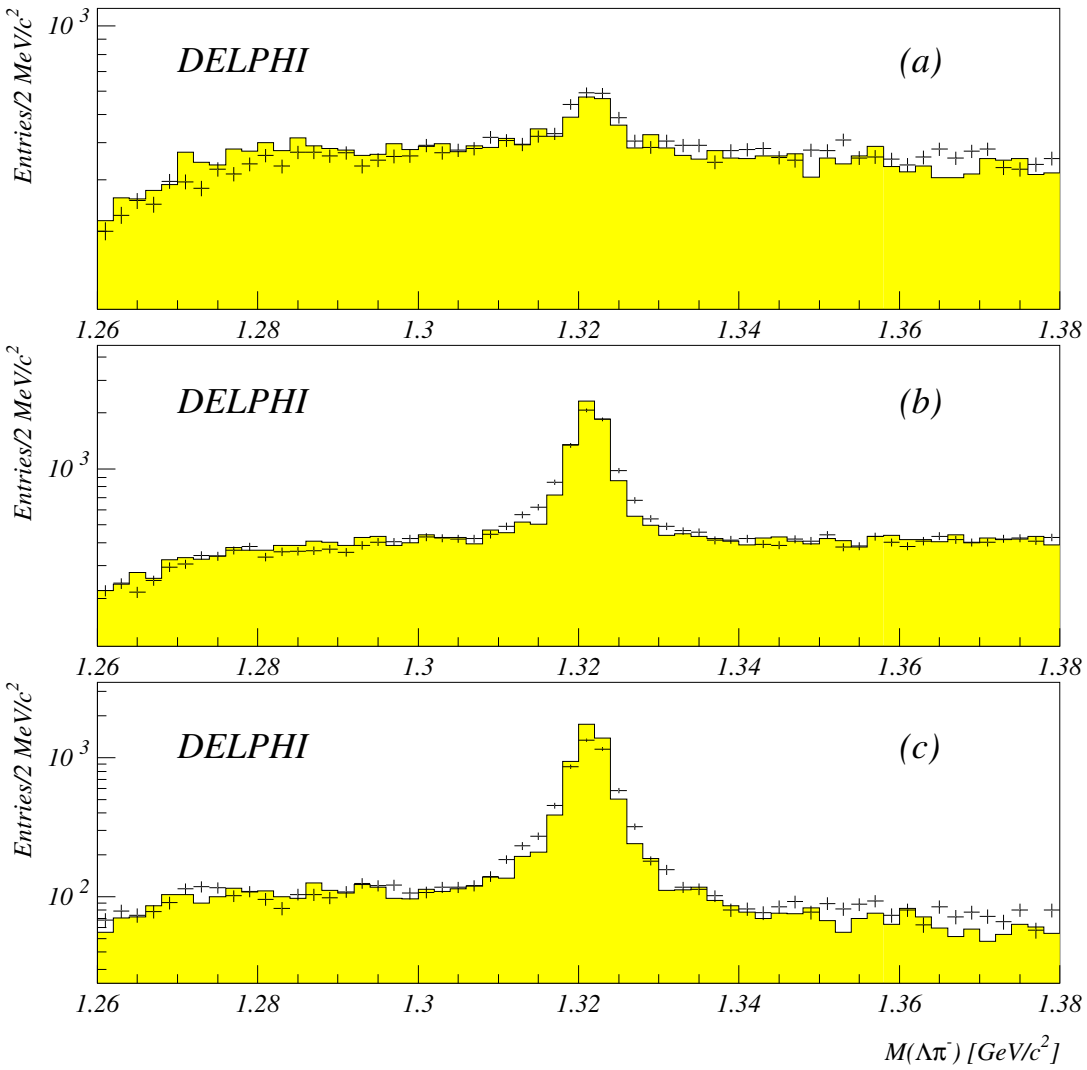

Figure 1: The right-sign ($\Lambda\pi^-$ and $\overline{\Lambda}\pi^+$) mass distribution with the Ξ (Ξ^- and $\overline{\Xi}^+$ added) signals in different χ^2 probability bins for data and simulation. The data are represented by the points with error bars and the simulation by the histograms, which are normalized to the same number of entries: **(a)** shows the Ξ signal without any other cuts applied for events with a χ^2 fit probability below 1%, **(b)** shows the Ξ signal without any other cuts applied for events with a χ^2 fit probability above 1%, **(c)** shows the Ξ signal after all cuts given in the text were applied for events with a χ^2 fit probability above 1%.

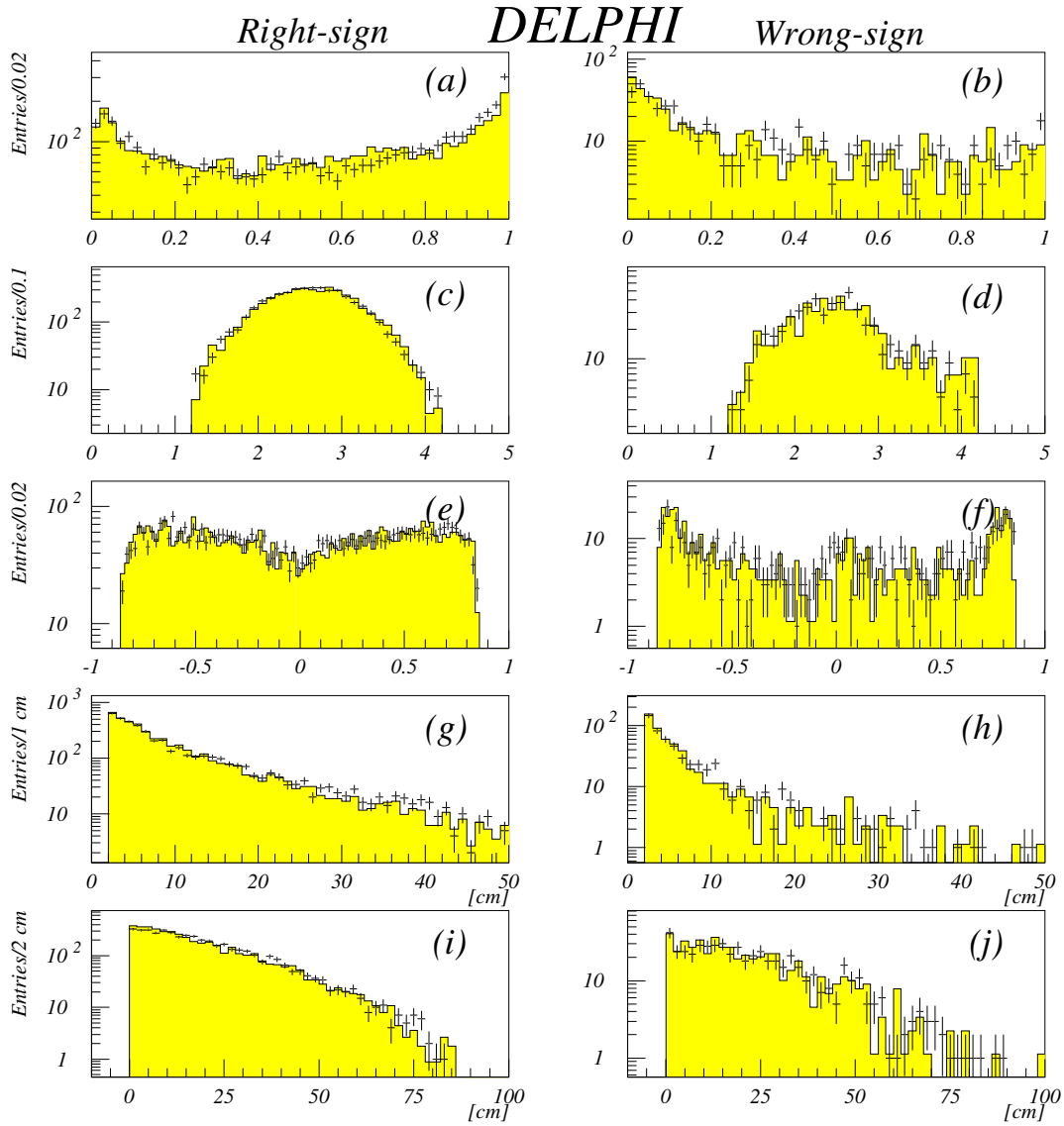

Figure 2: All the variables used in the Ξ selection for candidates in the mass interval $M_\Xi \pm 5$ MeV/c^2. The histograms are from the simulation and the points with error bars are the data. The years 1992 to 1995 have all been added, both for data and simulation. The simulation histograms are normalized to the data ones. All variables are shown for right-sign ($\Lambda\pi^-$ and $\overline{\Lambda}\pi^+$) and wrong-sign ($\Lambda\pi^+$ and $\overline{\Lambda}\pi^-$) combinations after all cuts have been made: **(a,b)** χ^2 probability, **(c,d)** $\xi = -\ln(p_\Xi/p_{beam})$, **(e,f)** cosine of the polar angle θ of the Ξ momentum, **(g,h)** flight distance of the Ξ in the xy plane, **(i,j)** distance in the xy plane between the Λ and Ξ decay points.

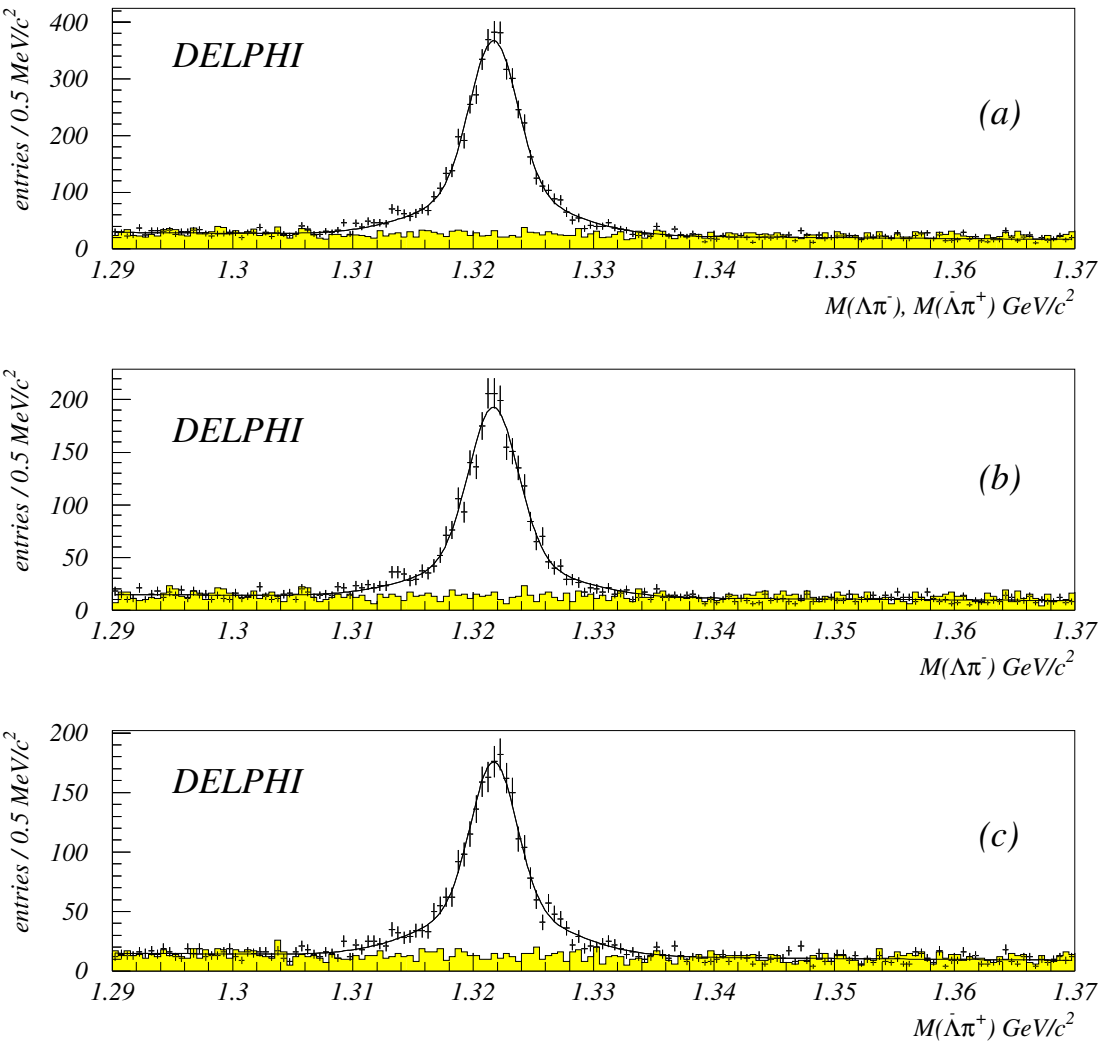

Figure 3: 1992-1995 data: **(a)** the Ξ^- and $\overline{\Xi}^+$ sample, **(b)** the Ξ^- sample, **(c)** the $\overline{\Xi}^+$ sample, The points with error bars show the right-sign ($\Lambda\pi^-$, $\overline{\Lambda}\pi^+$) combinations. The wrong-sign ($\Lambda\pi^+$, $\overline{\Lambda}\pi^-$) combinations are shown as the shaded histograms. The curves show the fits to the Ξ mass distributions described in the text (solid line).

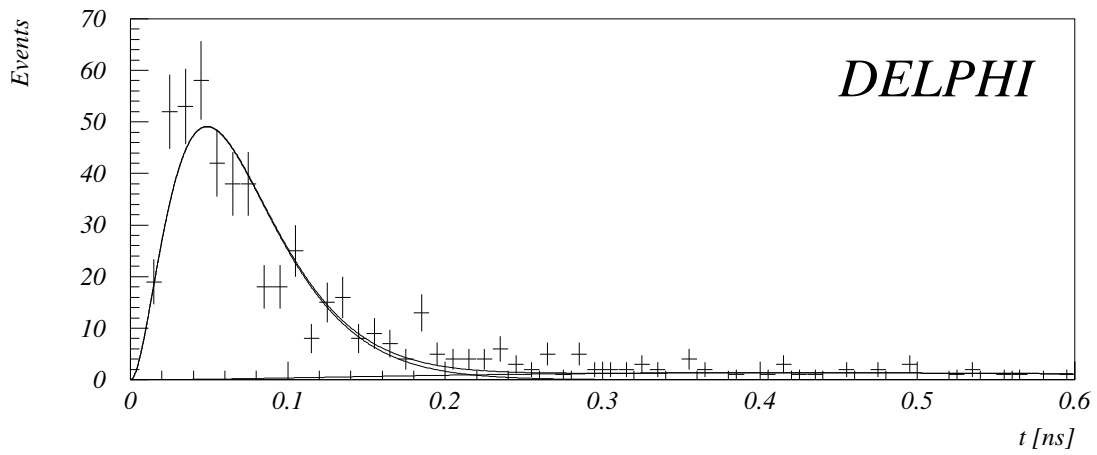

Figure 4: The observed time distribution in the wrong-sign sample for 1992-1995 data. The two lower curves are the b-functions described in the text. Their sum, used to describe the combinatorial background, is also shown. Only events with times larger than 0.04 ns were used in the fit.

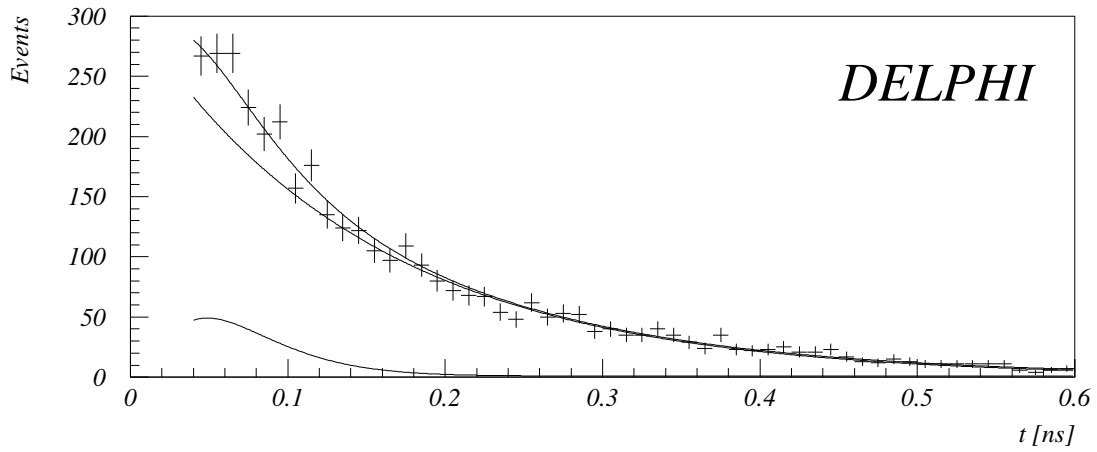

Figure 5: The observed time distribution in the right-sign sample for 1992-1995 data. The lowest curve is the estimate of the contribution from combinatorial background events, obtained by fitting the wrong-sign combinations. The middle curve is the estimate of the contribution of Ξ^- and $\overline{\Xi}^+$ decays. The upper curve represents the fit to the observed time distribution, *i.e.* the sum of the two lower distributions.

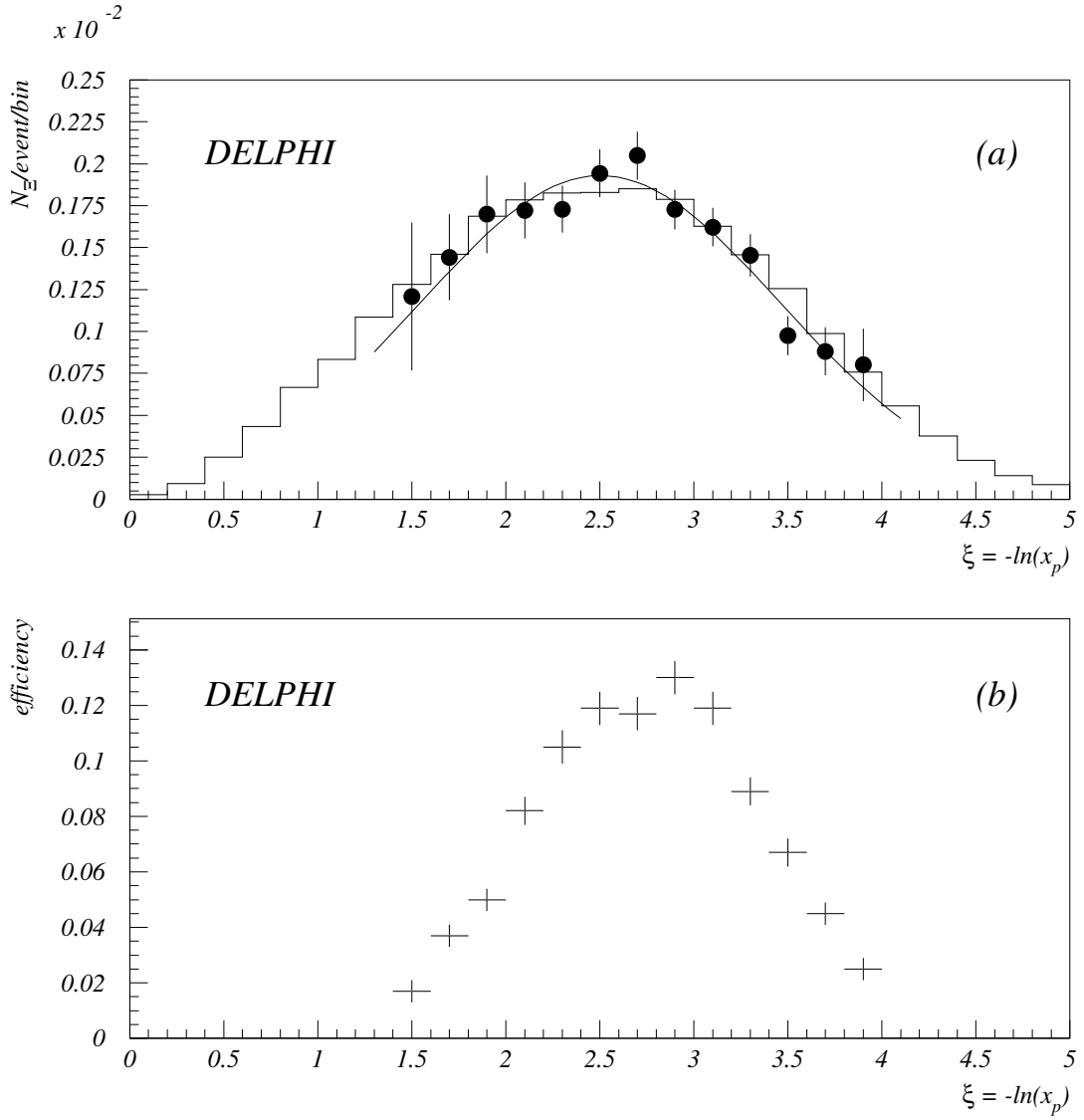

Figure 6: **(a)** Efficiency-corrected distribution of $\xi = -\ln x_p$: the points with error bars represent the measured ξ distribution, a fit to a Gaussian function is superimposed, and the JETSET ξ spectrum is shown as the solid histogram. **(b)** The Ξ^- reconstruction efficiency as a function of ξ.